Parametric Aeroelastic Stability Analysis of a Generic X-Wing Aircraft

Jessica A. Woods* and Michael G. Gilbert†
NASA Langley Research Center, Hampton, Virginia
and
Terrence A. Weisshaar‡
Purdue University, West Lafayette, Indiana

This paper discusses the dynamic aeroelastic stability of a generic X-wing aircraft configuration. The analysis model includes rigid-body degrees of freedom and unsteady aerodynamic forces generated using the doublet lattice method. Design parameters are varied to evaluate the trends in dynamic aeroelastic stability. X-wing rotor blade sweep angle, ratio of blade mass to total vehicle mass, blade structural stiffness cross coupling, and vehicle center of gravity location were parameters considered. The typical instability encountered is "body-freedom" flutter involving a low-frequency interaction of the first elastic mode and the aircraft short period mode. In most parametric cases, those cases having the least static longitudinal stability demonstrated the highest flutter dynamic pressures. As mass ratio was increased, the flutter boundary decreased. The decrease was emphasized as center of gravity location was moved forward. As sweep angle varied, it was observed that the resulting increase in forward-swept blade bending amplitude relative to aft blade bending amplitude in the first elastic mode had a stabilizing effect on the flutter.

Nomenclature

$[A_i]$ = constant coefficients
b = wing semichord
$[B_i]$ = aerodynamic lag coefficients
$[C']$ = generalized damping matrix
$[\hat{C}]$ = modified damping matrix
EI = bending stiffness
$[F]$ = system matrix
GJ = torsional stiffness
$[I]$ = identity matrix
j = $\sqrt{-1}$
$\tilde{K}$ = stiffness cross coupling
k = reduced frequency, $(\omega b)/V$
$[\hat{K}]$ = modified stiffness matrix
$[K']$ = generalized stiffness matrix
L = number of aerodynamic lags
L_b = blade length
$[M']$ = generalized mass matrix
m_b = blade mass
m_f = fuselage mass
m_r = blade to vehicle mass ratio
$[\hat{M}]$ = modified mass matrix
q = dynamic pressure
q_{f0} = nominal flutter dynamic pressure
q_f = flutter dynamic pressure
$[Q]$ = aerodynamic force matrix
s = Laplace variable
V = freestream velocity
W_i = aerodynamic lag term
$\bar{x}_{cg}$ = center of gravity location, x/L_b
$\bar{x}_{ac}$ = aerodynamic center location
z = state vector
β_i = aerodynamic lags
η = generalized coordinate
ω = oscillation frequency
ω_{n10} = nominal first elastic mode natural frequency
ω_{n1} = first elastic mode natural frequency
ω_{n2} = second elastic mode natural frequency
Ψ = nondimensional stiffness cross coupling parameter
Ψ_f = stiffness cross coupling in forward blade
Ψ_a = stiffness cross coupling in aft blade
Λ = sweep angle
Λ_m = sweep angle indicating minimum flutter dynamic pressure
Λ_{tr} = transition sweep angle

Presented as Paper 89-1385 at the 30th Structures, Structural Dynamics and Materials Conference, Mobile, Alabama, April 3-5, 1989; received June 7, 1989; revision received Dec. 4, 1989.

*Aerospace Engineer, Aeroservoelasticity Branch, Structural Dynamics Division. Member AIAA.
†Aerospace Engineer, Aeroservoelasticity Branch, Structural Dynamics Division. Senior Member AIAA.
‡Professor, School of Aeronautics and Astronautics Engineering. Associate Fellow AIAA.

Introduction

THE X-wing aircraft is a unique vehicle configuration combining the vertical takeoff advantages of a helicopter and the high-speed forward flight capability of a fixed wing aircraft. The aircraft concept utilizes a four-bladed, bearingless rotor system capable of operation in three flight phases. Vertical takeoff and hover with rotating blades comprise the first flight phase. The second phase is a conversion mode in which the blade rotation slows to a stop. In the third phase, the stopped rotor blades act as fixed wings for high-speed forward flight.[1] Two of the blades are swept forward and two are swept aft, symmetrically. From this configuration, the aircraft has become known as the "X-wing."

In each of these phases of flight, circulation control blowing provides a mechanism for augmenting and controlling lift.[2] Essentially, circulation control is achieved by blowing a sheet of air through spanwise slots over the trailing edges of Coanda airfoils. Because these quasielliptical airfoils have rounded trailing edges, the flow remains attached and the airfoils' stagnation point is relocated. Thus, lift and stability can be modulated by controlling the strength and spanwise distribution of blowing.

It has been analytically and experimentally demonstrated in the past that fixed wing aircraft with forward-swept wings

exhibit substantial coupling between elastic and rigid-body vibration modes. This symmetric, low-frequency flutter condition is commonly referred to as "body-freedom" flutter and is a coupling of wing bending and rigid-body pitch and plunge motions.[3] Because of the similarities between this configuration and the X-wing in a fixed rotor mode, it is likely that such an instability will be characteristic of the vehicle.

Several studies have focused on the aeroelastic stability of this unique configuration. For instance, in 1981, Gimmestad[4] conducted a study of a preliminary X-wing design. The analysis model included vehicle rigid-body degrees of freedoms but did not involve circulation control blowing. Gimmestad's results indicated that aft blade motion damps unstable forward blade motion through body freedoms until high velocities when the vehicle loses stability in pitch and an entire vehicle divergence results.

In 1987, Gilbert and Silva[5] evaluated the aeroelastic stability of an X-wing configuration that was to be used for flight testing. Their model also included rigid-body degrees of freedom and did not have circulation control blowing along the blades. Their study showed that with increasing airspeed, aeroelastic deformations of an X-wing configuration caused a forward shift in the aircraft aerodynamic center (a.c.) location and therefore a loss of static margin. Compared to Gimmestad's study, however, the divergence occurred at lower airspeeds, which is due, primarily, to lower blade natural frequencies. It was also concluded that no antisymmetric divergence or flutter modes exist.

More recently, Haas and Chopra[6] have analytically investigated an X-wing configuration with circulation control blowing but without rigid-body freedoms. At moderate angles of attack and high blowing levels, a single degree of freedom flutter involving the first blade bending elastic mode occurs. The instability is due to the airfoil section's negative lift curve slope at these high blowing levels. It is emphasized that the flutter is not dynamic stall, as there is no flow separation. At reduced blowing levels, classical bending-torsion flutter is observed. The highly rigid vehicle experiences classical bending-torsion flutter and static divergence at very high airspeeds.

The purpose of this study is to determine the dynamic aeroelastic behavior of a generic X-wing aircraft configuration with rigid-body degrees of freedoms. As a basis for the study, a generalized X-wing aeroelastic model is developed for a vehicle in the stopped rotor mode. The model has characteristics similar to the X-wing rotor studied in Ref. 5. Composite-beam finite elements were used to model the X-wing blade structure, and the doublet lattice lifting surface theory[7] is used to calculate the unsteady aerodynamics. Variations in both structural and aerodynamic parameters are made to determine trends in the flutter behavior. The analysis uses only symmetric vibration modes, and circulation control blowing is not modeled.

Aeroelastic Model Development

Equations of Motion

The equations of motion for a free-flying aeroelastic vehicle can be expressed in terms of vehicle rigid-body and elastic vibration modes[8] as

$$\{[M']s^2 + [C']s + [K'] + q\,[Q(s)]\}[\eta(s)] = 0 \tag{1}$$

Structural Model

To model the generic X-wing configuration, a structural half-model was developed using beam finite elements. The model was general in the sense that parametric variations could easily be made in the sweep angle, mass, and stiffness properties. The beam element was incorporated into Engineering Analysis Language (EAL) for a free vibration analysis of the model.[9]

The finite element used in this study was developed to model beams having the characteristics of bending-torsion stiffness cross coupling and is described by elemental mass and stiffness matrices, which are defined in Ref. 10. Both elemental matrices involve a nondimensional parameter Ψ, which describes the stiffness cross coupling. It is defined by Weisshaar[11] as

$$\Psi = \pm\sqrt{\tilde{K}^2/EI \cdot GJ} \tag{2}$$

where $\tilde{K}$ denotes stiffness cross coupling between bending and torsional deformations. Limits on Ψ are derived from the energy requirement that a stiffness matrix must be positive semidefinite

$$\left|\begin{bmatrix} EI & \tilde{K} \\ \tilde{K} & GJ \end{bmatrix}\right| \geq 0.0 \tag{3}$$

or equivalently

$$EIGJ - \tilde{K}^2 \geq 0.0$$

which implies

$$-1 \leq \Psi \leq 1$$

A positive value of Ψ indicates that upward (positive) beam bending induces a leading-edge uptwist or "washin." A negative value of Ψ indicates that upward (positive) beam bending induces a leading-edge downtwist or "washout." A value of zero for Ψ represents the absence of stiffness cross coupling. Physically, Ψ is determined by the composite ply orientation within a given composite laminate.

The actual X-wing structural half-model takes advantage of the vehicle's symmetry while in the fixed rotor mode. It consists of two untapered blades, one with forward sweep and one with aft sweep, each modeled by 10 finite elements. The specific nodal layout and some parameter definitions are illustrated in Fig. 1.

Vehicle center of gravity (c.g.) location, also shown in Fig. 1, is determined by the two mass components of the X-wing half-model. One mass component is the set of two blades. The other is an attached mass simulating the fuselage and is positioned at varying locations along the vehicle's longitudinal axis. The element used to link fuselage and blade motion is massless and rigid.

Some typical mode shapes from the vibration analysis are presented in Fig. 2. Only the frequencies and vertical displace-

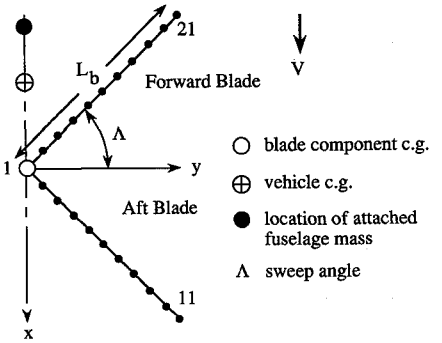

Fig. 1 Nodal layout and parameter definition.

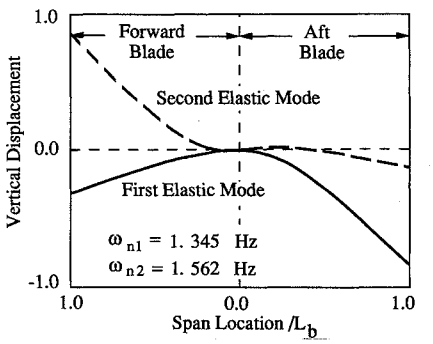

Fig. 2 Mode shapes and frequencies for nominal case.

ments of the first two elastic modes are shown. In general, the modes computed in this study did not demonstrate torsion along the blade at low frequencies unless the structure involved stiffness cross coupling. Motion of the forward-and aft-swept blades is not symmetric with respect to the y axis due to the forward c.g. location.

Aerodynamic Model

The X-wing half-model is further developed by defining aerodynamic lifting surfaces. Combining these planform geometries with the free vibration mode shapes, an unsteady aerodynamic analysis can be conducted to determine generalized aerodynamic forces acting on the vehicle at various reduced frequencies.

Several assumptions have been made in the aerodynamic calculations. First, it is assumed that the doublet lattice linear aerodynamic theory is sufficient to model X-wing aerodynamics. An important implication is that interference between the forward-and aft-swept blades is limited to downwash effects. Second, because symmetric structural vibration mode shapes are used for the analysis, the aerodynamics are also specified as symmetric about the x-z plane. Finally, circulation control blowing has not been modeled. Although it was shown by Haas and Chopra[6] that the strength and spanwise distribution of blowing directly affect the static and dynamic aeroelastic vehicle responses, it is assumed in the present study that there is no circulation control along the blades other than a small amount that serves to keep the flow attached to the blade.

Unsteady generalized aerodynamic forces in this investigation are computed using the doublet lattice method as available in Interaction of Structures, Aerodynamics and Controls (ISAC).[12] They are computed as tabulated functions of Mach number and reduced frequency k defined as $k = (\omega b)/V$, where ω is the oscillation frequency, b one-half the blade chord length, and V the velocity. The aerodynamic forces are computed for harmonic motion and are extended to arbitrary motion using a rational function approximation method described below. For this study, generalized aerodynamic forces are computed for Mach = 0.3. A representative doublet lattice box layout is shown in Fig. 3.

The rational function approximation to the tabulated aerodynamic forces is made in the form[8]

$$[Q(s)] = [A_0] + [A_1]\left(\frac{bs}{V}\right) + [A_2]\left(\frac{bs}{V}\right)^2 + \sum_{i=1}^{L} \frac{[B_i]s}{\left(s + \frac{V\beta_i}{b}\right)} \tag{4}$$

$[A_0]$, $[A_1]$, $[A_2]$, and the $[B_i]$ are real and are computed using a least-squares fit to the tabulated generalized aerodynamic forces for the case of harmonic motion, $s = j\omega$. The lags β_i are arbitrarily chosen to be within the reduced frequency range under investigation and provide a good approximation for $s = j\omega$. The approximations are constrained to be an exact fit to the tabulated aerodynamic forces at $k = 0$ in order to define as accurately as possible forces generated by rigid-body modes and the steady-state aerodynamics. In this study, there are four aerodynamic lag coefficients, $\beta = 0.1$, 0.15, 0.25, 0.4, and 10 values of reduced frequency in the range of $k = 0$ to $k = 1$.

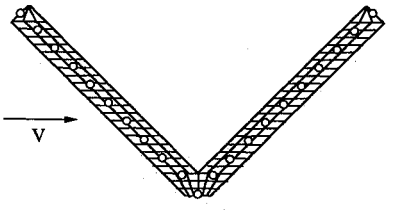

Fig. 3 Typical panel layout showing structural node locations.

State Space Formulation

With the aerodynamics in functional form and the structural matrices defined, the equation of motion, Eq. (1), can be rewritten in state space form for stability analysis as shown in the Appendix.

Aeroelastic Stabilty Analyses

Analysis Method

With the development of generalized X-wing model, parametric variations will be made and the vehicle stability studied. A parametric variation is defined as the changing of a vehicle dimension, stiffness, or mass property while fixing the other system parameters to nominal values. Each specific combination of parametric and nominal values is referred to as a "configuration." In this study, c.g., sweep angle, blade-to-vehicle mass ratio, and stiffness cross coupling are chosen to be the system parameters. The nominal value of each parameter is listed in Table 1.

The ISCA stability analysis for each case involves determining the eigenvalues of the associated system matrix $[F]$, Eq. (A6) in the Appendix, over a range of velocities. A complex eigenvalue or root is stable when the real part is less than zero. A positive real part implies instability, i.e., negatively damped, oscillatory motion of the associated rigid-body or elastic mode. A real root is stable if it is less than zero and unstable if it is greater than zero. To illustrate the trend in these roots as a function of velocity, eigenvalues are presented in a root loci format similar to the root loci format used in control system analysis.

In this study, 12 symmetric mode shapes, including the rigid-body pitch and plunge motions, were used for the stability analysis of each configuration.

Nominal Configuration

To illustrate typical trends in X-wing stability, the root locus of the nominal forward c.g. case ($\bar{x} = -0.15$) is presented in Fig. 4. The velocity variations are approximately 30 mph intervals between 30 and 600 mph. Since only the first two elastic modes and rigid-body modes show any tendency towards instability, higher frequency modes have not been shown. First and second elastic mode roots move away from each other; the first mode frequency decreases while the second mode frequency increases. Coupling of the first elastic mode with the vehicle short-period mode is defined as a body-freedom flutter condition.

Mass Ratio Variation

Mass ratio m_r is defined for the half-model as

$$m_r = m_b/(m_b + m_f) \tag{5}$$

where m_f is one-half the attached fuselage mass and m_b is the mass of two blades. The nominal value of m_r is 0.25. Configurations are examined at $m_r = 0.15$, 0.25, 0.35, 0.45, and 0.55, in each case at two forward c.g. locations, $\bar{x} = -0.15$ and $\bar{x} = -0.3$.

Mass ratio is varied by changing the blade mass per unit length while holding the total vehicle mass constant. Pitch inertia and vehicle c.g. location are also held constant. To keep the vehicle pitch inertia constant, the fuselage inertia is modified as m_b varies. To maintain a constant c.g. location, the location of the attached fuselage mass is varied.

Velocity root loci are, for most of the cases, similar to those shown in Fig. 4. First and second elastic mode roots move

Table 1 Nominal parameter values

Λ	45 deg	sweep angle
m_r	0.25	blade-to-vehicle mass ratio
Ψ	0.0	stiffness cross coupling in forward and aft blades
$\bar{x}$	−0.15	c.g. location

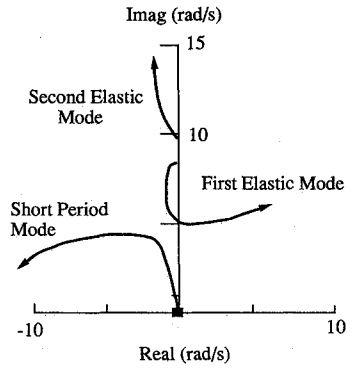

Fig. 4 Root locus for nominal case.

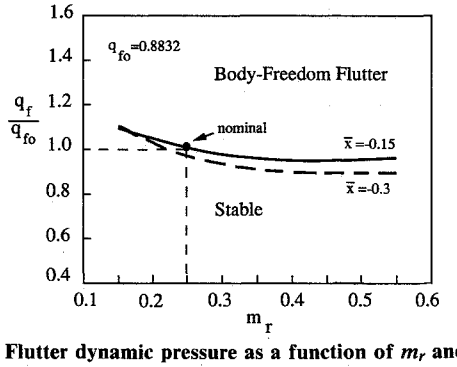

Fig. 5 Flutter dynamic pressure as a function of m_r and $\bar{x}\ c_g$.

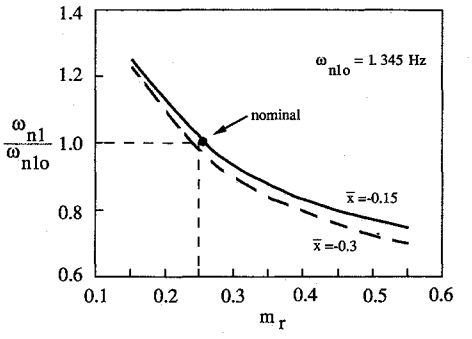

Fig. 6 Variation of natural frequency with $\bar{x}\ c_g$ and m_r.

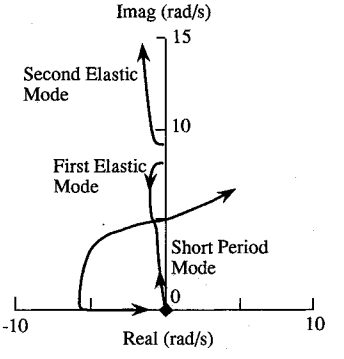

Fig. 7 Root locus of $\Lambda = 30$ deg, $\bar{x}\ c_g = -0.3$ configuration illustrating interaction of short period and first elastic modes.

away from one another as velocity increases; interaction between the short-period and first elastic roots results in the latter roots moving into the right-half plane. The exception is the case with $m_r = 0.15$ and $\bar{x} = 0.15$. Contrary to the typical trend, as velocity increases, the short-period roots are driven into the right-half plane whereas the first elastic mode roots are forced into the left-half plane. The instability mode, however, is still body-freedom flutter.

Several interesting results were obtained from the stability analyses. These results are summarized in Fig. 5, which presents the flutter dynamic pressure as a function of mass ratio. Figure 5 shows that at $m_r = 0.15$, flutter boundaries for $\bar{x} = -0.15$ and $\bar{x} = -0.3$ cases intersect. Further investigation showed that these two cases are essentially the same configuration. With small mass ratios, the fuselage is massive enough to create a "near-clamped" fuselage condition so that c.g. location is no longer a factor. Furthermore, since the structural characteristics of the blades are the same for a given m_r at any c.g. location, the first two elastic mode natural frequencies are nearly identical.

As mass ratio increases, the effect of c.g. location is to separate the flutter boundaries. Cases with the more forward c.g. locations have the lower flutter dynamic pressures. In addition, Fig. 5 shows that an overall decrease in flutter dynamic pressure q_f occurs as mass ratio increases. This happens because the blade first mode natural frequencies decrease by as much as 50% when m_r is increased from 0.15 to 0.55, as shown in Fig. 6. This decrease causes the short-period and first elastic modes to interact at increasingly lower dynamic pressures. The decrease occurs because blade mass per unit length, which is inversely proportional to the square of natural frequency, increases with m_r.

Sweep Angle Variation

As shown in Fig. 1, blade sweep angle is defined as one-half the relative angle between forward- and aft-swept X-wing rotor blades. The nominal value is $\Lambda = 45$ deg. Configurations examined are $\Lambda = 15$, 30, 45, 60, and 75 deg, each with c.g. locations $\bar{x} = -0.15$ and -0.3. Velocity root loci for the various sweep configurations are similar to those shown in Fig. 4. The first elastic mode and short-period mode roots interact to create a body-freedom flutter condition. However, as Λ increases, a transition occurs. The $\Lambda = 15$ deg cases have short-period mode roots moving into the right-half plane at flutter, whereas the $\Lambda = 45$ deg cases have first elastic mode roots moving into the right-half plane. This transition is shown in Fig. 7, a root locus for the configuration described by $\Lambda = 30$ deg and $\bar{x} = -0.3$. There is a velocity at which the first elastic mode roots and short-period mode roots become indistinguishable. It is unclear which roots pass into the right-half plane. A similar transition also occurs in the $\bar{x} = -0.15$ cases but at a sweep angle not investigated ($15 \text{ deg} < \Lambda < 30$ deg).

Structural vibration mode shapes for representative cases $\Lambda = 15$ deg and 45 deg, both with $\bar{x} = -0.15$, are compared in Fig. 8. In the $\Lambda = 45$ deg case, both blades move together in the first elastic mode with the aft blade having a larger relative amplitude. As Λ decreases below 45 deg, a "modeswitch" occurs, and in the extreme case of $\Lambda = 15$ deg, forward and aft blades move opposite to one another, although the aft blade still has a larger relative amplitude. Thus, at some transition sweep angle, denoted as Λ_{tr}, the first elastic mode involves, primarily, bending of the aft blade and no relative forward-blade bending. The transition sweep angle increases with forward motion of the c.g. For the $\bar{x} = -0.15$ cases, $\Lambda_{tr} \approx 30$ deg, whereas for the $\bar{x} = -0.3$ cases, $\Lambda_{tr} \approx 45$ deg.

Results of the dynamic stability analyses are shown in Fig. 9. In both the $\bar{x} = -0.15$ and the $\bar{x} = -0.3$ cases, minimums in flutter boundaries are present. The sweep angle at which these minimums occur is denoted by Λ_m. In the $\bar{x} = -0.15$ case, $\Lambda_m \approx 38$ deg and in the $\bar{x} = -0.3$ case, $\Lambda_m \approx 45$ deg.

Cases with sweep angles greater than Λ_m demonstrate flutter trends consistent with those observed over m_r variations. Specifically, the flutter dynamic pressures are higher for cases with the more aft c.g. locations. In addition, for a given c.g. location, the static margin ($\bar{x}_{cg} - \bar{x}_{ac}$) was observed to decrease slightly with increasing sweep angle. This is associated with an increase in the flutter dynamic pressure. It is noted, also, that mode shapes are similar to those observed over m_r variations.

Cases with sweep angles less than Λ_m demonstrate the reverse trend. An increasing static margin is associated with an increasing flutter dynamic pressure. It is likely that this trend reversal is due to the transition in mode shapes from those observed over m_r variations. The increased forward blade bending in the first elastic mode appears to be stabilizing the flutter condition.

Aeroelastic Tailoring

The final objective of this study was to find a means of delaying or eliminating body-freedom flutter of the X-wing. For this purpose, aeroelastic tailoring through the use of stiffness cross coupling was investigated. This coupling was incorporated independently into the forward- and aft-swept blades of the nominal configuration, and the values of Ψ considered were $\Psi = -0.5, -0.25, 0.25$, and 0.5.

Velocity root loci for the tailored X-wing configurations were found to be similar to the typical root locus shown earlier in Fig. 4. All cases experienced body-freedom flutter as a result of short-period and first elastic mode interaction.

The vehicle flutter dynamic pressure as a function of blade stiffness cross coupling is shown in Fig. 10. In this figure, one flutter boundary is associated with cases in which Ψ changes only on the forward blades and remains zero in the aft blades. The other curve represents a boundary for cases with Ψ changes in the aft blade while forward-blade cross coupling is zero. It is seen that stiffness tailoring of the forward-swept blades has a small effect on the flutter stability of the parametric case evaluated. The result is not surprising because the forward-swept blades have a small bending amplitude relative to the aft-blade bending amplitude in the first elastic mode of this configuration. Thus, changes in aerodynamic loading due to coupling-induced washin or washout of forward blades are small when compared to the aft-blade loads.

With negative cross coupling washout, in the aft-swept blades, the natural tendency of the blades to washout during bending is magnified. As a result of the decreased aerodynamic loads, the static margin is decreased. It has been shown previously that a decrease in static margin increases flutter dynamic pressure. The addition of positive cross coupling, washin, in the aft blades causes the below the uncoupled flutter dynamic pressure. The natural tendency of the blade to washout has been dominated by stiffness-induced washin. As a result of the increased blade loading, static margin is increased and flutter dynamic pressure declines.

There exists a point of diminishing returns, where further increases in Ψ lead to decreases in q_f. This may be explained by considering the decrease in first mode natural frequencies as the magnitude of Ψ increases. The frequencies change slightly because both the mass matrix elements and the bending stiffness are functions of Ψ. As the magnitude of Ψ increases, variations in the mathematical model increasingly affect the system characteristics. In this case, the lower frequencies allow for interaction of short-period and first elastic mode roots at lower dynamic pressures or q_f.

Pitch Moment Effects

An analysis involving vehicle stability as a function of c.g. location yielded some interesting insight into vehicle stability trends. The locations considered were $\bar{x} = -0.3, -0.15, -0.075, 0.0$, and 0.15. Figure 11 summarizes the results. The upper curve defines a boundary above which body-freedom flutter occurs. For $\bar{x} < -0.15$, flutter dynamic pressure is slightly less than that of the nominal case. It increases dramatically as the c.g. is moved aft, which is effectively decreasing the static margin. The lower curve is a restabilization boundary of the vehicle divergence condition that is consistently observed in the cases where the initial a.c. location is forward of the vehicle c.g.

As illustrated in the root locus of an initially unstable case, shown in Fig. 12, the short period mode root lies along the positive real axis and moves outward with increases in velocity. The root eventually reaches a limit and begins to move to the left along the real axis. Restabilization of the root is followed at higher velocities by the body-freedom flutter condition described previously.

Insight is gained by considering the first elastic mode shape as a funciton of c.g. location, shown in Fig. 13. In the forward c.g. locations, aft-swept blade bending amplitude is much

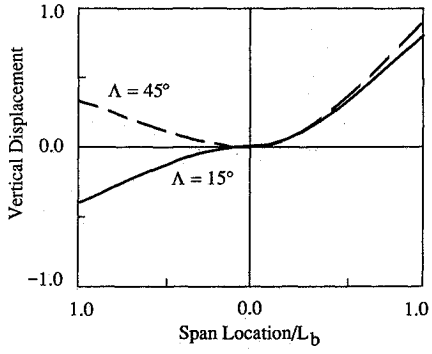

Fig. 8 Variation of first elastic mode as Λ increases for configurations with $\bar{x}\ c_g = -0.15$.

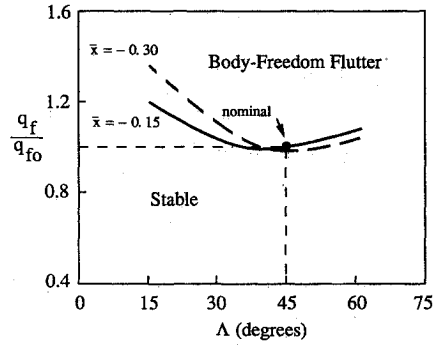

Fig. 9 Variation of flutter boundary with changes in sweep angle.

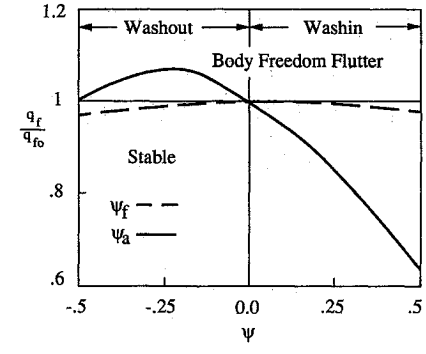

Fig. 10 Variation of flutter dynamic pressure with Ψ as it is applied independently to the forward-swept blade (Ψ_f) and to the aft-swept blade (Ψ_a).

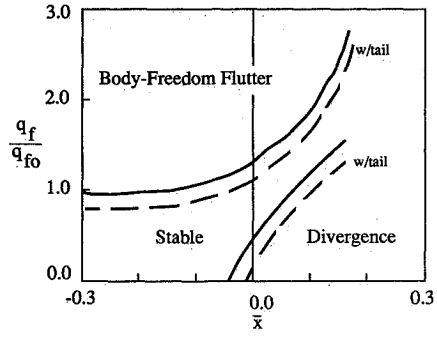

Fig. 11 Stability boundaries as funciton of $\bar{x}\ c_g$, including the effect of a tail.

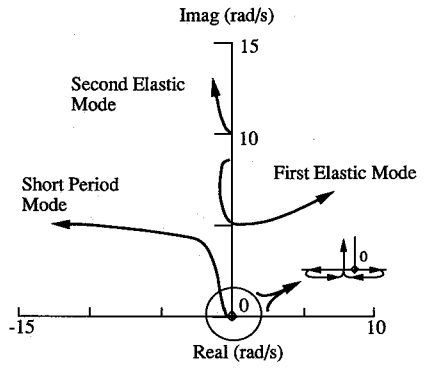

Fig. 12 Root locus illustrating restabilization of the short period mode roots along the real axis.

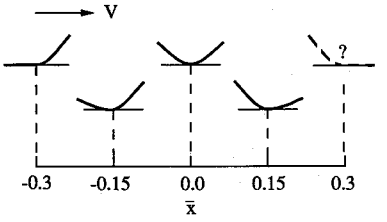

Fig. 13 Transition of first elastic mode vertical displacement as a funciton of $\bar{x}$ c_g.

larger than forward-swept blade bending amplitude. At $\bar{x} = 0.0$, blades bend together with the same amplitude because the vehicle is longitudinally symmetric. As the c.g. is moved aft, forward blade bending becomes the dominant bending amplitude. Herein lies the possibility of vehicle divergence for the statically unstable cases. At low velocities, forward-swept blades begin to develop larger air loads due to aeroelastic washin. Because forward blade bending amplitude is significantly larger than aft blade bending amplitude in these cases, there is insufficient nose-down pitch moment generated by the aft blades to counteract nose-up moments due to the forward-blade air loads. Thus, the X-wing experiences a vehicle divergence instability characterized by an aperiodic upward pitch. As velocity increases, forward-swept blade inertial load[13] and aft blade air loads increase, theoretically restabilizing the vehicle. One implication of this is that stability augmentation of the divergent motion may only be required at low velocities.

Similarly, in the statically stable cases, forward-swept blade loads serve to counteract unstable aft blade loads. At the most forward c.g. location, the mode shapes involve large aft blade bending amplitude relative to forward blade bending amplitude. These configurations demonstrate the lowest flutter dynamic pressures. As c.g. moves aft, there is an increase in the relative forward blade bending amplitudes as well as a decrease in the static margin, both of which cause reductions in the vehicle pitch moment. This indicates that increased forward blade motion has a stabilizing effect on the apparently unstable aft blade motion. Further, the body-freedom flutter dynamic pressures increase. Thus, the same decrease in vehicle pitch moment that increases the likelihood of vehicle divergence decreases the likelihood of body-freedom flutter.

This statement is supported by aeroelastic tailoring results. When aft blades experience cross-coupling induced washout, an overall decrease in pitch moment occurs. Figure 10 shows the associated increase in flutter dynamic pressure.

It is noted that the tendency to have an increasing body-freedom flutter dynamic pressure with a decreasing longitudinal static stability margin has been shown in two previous studies of unconventional aircraft. One study involved flutter of the X-29 forward-swept wing aircraft,[3] and the other involved flutter of a tailless sailplane.[14] As another point of interest, the addition of a tail would probably increase nose-down pitching moment and therefore would shift the dynamic divergence curve to the right as shown in Fig. 11. The flutter boundary, however, would drop because increases in pitch moment have been shown to be destabilizing.

Conclusions

The X-wing's typical aeroelastic instability while in the fixed rotor mode is body-freedom flutter, a low-frequency interaction between the first elastic mode and the short period mode. Cases with positive static margins demonstrated the highest flutter dynamic pressures. As the ratio of X-wing rotor-to-fuselage mass increased, the flutter dynamic pressures decreased. This trend is due to a decrease in first elastic mode natural frequency with increasing mass ratio. The decrease in flutter dynamic pressures was more pronounced as c.g. location moved forward. An increase in forward-swept blade bending amplitude relative to aft-swept blade bending amplitude in the first elastic mode due to sweep angle variations had a stabilizing effect on the flutter boundaries at two different c.g. locations. Finally, negative stiffness cross coupling or washout incorporated into the aft blades caused the flutter dynamic pressure to increase above the uncoupled flutter dynamic pressure. Positive cross coupling in the aft blade or washin was destabilizing. In the forward-swept blades, stiffness cross coupling had little effect on stability for the parametric case evaluated. Finally, it was concluded that rigid-body freedoms allow a stabilizing interaction between the motions of the forward- and aft-swept blades.

Appendix: State Space Model

Substituting the aerodynamic approximation, Eq. (3), into Eq. (1) yields[8]

$$\left\{[\hat{M}]s^2 + [\hat{C}]s + [\hat{K}] + \sum_{i=1}^{L} [W_i]s\right\}\{\eta(s)\} = 0 \qquad \text{(A1)}$$

where

$$[\hat{M}] = [M'] + q[A_2](b/V)^2$$

$$[\hat{C}] = [C'] + q[A_1]\,(b/V)$$

$$[\hat{K}] = [K'] + q[A_0]$$

and where

$$[W_i] = \frac{q[B_i]}{s + [(V\beta_i)/b]}$$

First-order state equations for the aerodynamic approximation terms can be obtained as

$$y_i = \frac{qs[B_i]\eta}{s + [(V\beta_i)/b]} = s[W_i]\eta \qquad \text{(A2)}$$

or

$$\{s + [(V\beta_i)/b]\}y_i = qs[B_i]\eta$$

which implies

$$sy_i = -[(V\beta_i)/b]\, Iy_i + qs[B_i]\eta \qquad \text{(A3)}$$

which is a first-order differential equation in y_i with I as the identity matrix.

A state vector z is defined for the system in which each aerodynamic lag contributes a state,

$$z^T = \{\eta^T\, s\eta^T\, y_1^T \ldots\ldots y_L^T\} \qquad \text{(A4)}$$

Thus, a state space representation of the system can be written by combining Eqs. (A3) and (A4).

$$sz = [F]z \tag{A5}$$

where

$$[F] = \tag{A6}$$

$$\begin{bmatrix} 0 & I & 0 & \cdot\cdot & 0 \\ -\hat{M}^{-1}\hat{K} & -\hat{M}^{-1}\hat{C} & -\hat{M}^{-1} & \cdot\cdot & -\hat{M}^{-1} \\ 0 & qB_1 & -\dfrac{\beta_1 VI}{b} & 0 & \cdot\cdot \\ \cdot & \cdot & 0 & \cdot & \\ \cdot & \cdot & \cdot & \cdot & \\ 0 & qB_L & \cdot & & -\dfrac{\beta_L VI}{b} \end{bmatrix}$$

In the time domain, the state space form is

$$\dot{z} = [F]z \tag{A7}$$

Acknowledgment

This research was conducted as part of Purdue University's Graduate Aeronautics Program at NASA Langley Research Center.

References

[1]Williams, R. M., "X-Wing and the Navy VSTOL Initiative," *AIAA Student Journal*, Vol. 19, No. 4, Winter 1981-82, pp. 26-34.

[2]Cheeseman, I. C. and Seed, A. R., "The Application of Circulation Control Blowing to Helicopter Rotors," *Journal of Royal Aeronautical Society*, Vol. 71, No. 848, July 1966.

[3]Weisshaar, T. A., Zeiler, T. A., Hertz, T. J., and Shirk, M. H., "Flutter of Forward Swept Wings, Analyses and Tests," AIAA Paper No. 82-0646, May 1982.

[4]Gimmestad, D.W., "A Preliminary Divergence and Flutter Evaluation of an X-Wing Aircraft," AIAA Paper No. 81-1671, Aug. 1981.

[5]Gilbert, M. G., and Silva, W. A. "The Effects of Aeroelastic Deformation of Unaugmented Stopped-Rotor Dynamics of an X-Wing Aircraft," AIAA Paper 87-2563CP, Aug. 1987.

[6]Haas, D., and Chopra, I., "Flutter of Circulation Control Wings," AIAA Paper 88-2345, April 1988.

[7]Geising, J. P., Kalman, T. P., and Rodden, W. P., "Subsonic Unsteady Aerodynamics for General Configurations, Part I: Direct Application of the Nonplanar Doublet Lattice Method," Air Force Flight Dynamics Lab., Wright-Patterson AFB, OH, TR-715, 1971.

[8]Mukhopadhyay, V., Newsom, J. R., and Abel, I., "A Method for Obtaining Reduced Order Control Laws for High Order Systems Using Optimization Techniques," NASA TP-1876, Aug. 1981.

[9]*Engineering Analysis Language*, Engineering Information Systems, Inc., San Jose, CA, 1983.

[10]Foist, B. L., "Aeroelastic Stability of Aircraft with Advanced Composite Wings," M.S. Thesis, School of Aeronautics and Astronautics, Purdue Univ., W. Lafayette, IN, Aug. 1982.

[11]Weisshaar, T. A., "Flutter and Divergence of Airfoils with Stiffness Cross-coupling," Purdue Univ., TR AAE-84-15.

[12]Peel, E., and Adams, W. M., "A Digital Program of Calculating the Interaction Between Flexible Structures, Unsteady Aerodynamics and Active Controls," NASA TM-80040, 1979.

[13]Bisplinghoff, R. L., and Ashley, H., *Principles of Aeroelasticity*, Dover, New York, 1962.

[14]Banerjee, J. R., "Flutter Characteristics of High Aspect Ratio Tailless Aircraft, Engineering Notes," *Journal of Aircraft*, Vol. 21, No. 9, Dec. 1984.